ASSESSMENT OF A NEW FLUENT MODEL FOR PARTICLE DISPERSION IN TURBULENT FLOWS

A. Dehbi
Paul Scherrer Institut, Department of Nuclear Energy and Safety,
Laboratory for Thermal-hydraulics
5232 Villigen, Switzerland

Abstract

In Lagrangian particle dispersion modeling, the assumption that turbulence is isotropic everywhere yields erroneous predictions of particle deposition rates on walls, even in simple geometries. In this investigation, the stochastic particle tracking model in FLUENT 6.2 is modified to include a better treatment of particle-turbulence interactions close to walls where anisotropic effects are significant. The fluid rms velocities in the boundary layer are computed using fits of DNS data obtained in channel flow. The new model is tested against correlations for particle removal rates in turbulent pipe flow and 90° bends. Comparison with experimental data is much better than with the default model. The model is also assessed against data of particle removal in the human mouth-throat geometry where the flow is decidedly three dimensional. Here, the agreement with the data is reasonable, especially in view of the fact that the DNS fits used are those of channel flows, for lack of better alternatives. The CFD Best Practice Guidelines are followed to a large extent, in particular by using multiple grid resolutions and at least second order discretization schemes.

1. Introduction

Particle-laden turbulent flows are common place in many and industrial, environmental and medical applications. Examples include nuclear fission products transport, drug delivery in human airways, fouling in compressor and turbine blades, pollutant control, etc. Therefore, an accurate description of particle transport and removal in turbulent flow fields is of great importance. Most of the investigations of particle-turbulence interactions have concentrated on unbounded flows where boundary layer wall effects are nonexistent. Comparatively, wall bounded flows have attracted much less attention. To a large extent, the deposition of particles onto the walls in turbulent flows is dictated by what happens in the boundary layer. Indeed, in many applications, turbulence can be approximated as being isotropic in the bulk; however, near the wall, it is known that the turbulent velocity fluctuations are not isotropic, and the rms of the normal component of velocity can be orders of magnitudes smaller than the streamwise or spanwise components. Hence, particles in the turbulent boundary layer are slowed considerably compared to what would be expected if the flow field were wholly isotropic.

Owing to the ever-increasing power of computer hardware, complex turbulent flows in nuclear safety applications are increasingly predicted using Computational Fluid Dynamics (CFD) tools. Given that fission product transport in reactor circuits is a major safety issue, it is only fitting that the behavior of particles also be addressed within the CFD methodology. In widely used CFD codes such as FLUENT [1], the turbulent dispersion of particles is predicted using a Lagrangian-type random walk model, while assuming turbulence is isotropic all the way to the wall. The latter assumption leads to large over-predictions of particle deposition rates even for simple flows such as those in pipes or parallel channels. In the following investigation, a model is presented whereby the default random walk model in FLUENT is modified to account for the anisotropic turbulence effects in the boundary layer.

2. Particle transport methods

There are two main families of methods to treat particle transport in fluid flows: Eulerian and Lagrangian. In the Eulerean or “two-fluid” approach, the particles are regarded as a continuous phase for which the conservation equations (continuity, momentum and energy) are solved in similar fashion to the carrier gas flow field. The Eulerean approach is particularly suitable for denser suspensions when particle-particle interactions are important and the particle feedback on the flow is too large to ignore. The main challenge facing Eulerian-type, two-fluid approaches resides in accurately defining the inter-phase exchange rates and closure laws which arise from the averaging procedures. In addition, the strong coupling between the phases renders the Eulerean approach quite delicate to handle, especially at boundaries where the solid phase may be removed.

In the second approach, called Lagrangian, the particles are treated as a discrete phase made of spherical particles which are dispersed in the continuous phase. The particle volume loading is usually assumed negligible, so that particles have no feedback effect on the carrier gas and particle-particle interactions are neglected. In the Lagrangian framework, the controlling phenomena for particle dispersion in the field are assessed using a rigorous treatment of the forces acting on the particle. In general, the detailed flow field is computed first, then a representatively large number of particles are injected in the field, and their trajectories determined by following individual particles until they are removed from the gas stream or leave the computational domain. Particle motion is extracted from the time integration of Newton’s second law, in which all the relevant forces can be incorporated (drag, gravity, lift, thermophoretic force, etc.). The Lagrangian approach is computationally intensive, because it entails tracking a large number of particles until stationary statistics are achieved. On the

other hand, the results of Lagrangian particle tracking are physically easier to interpret. Therefore, in the following investigation, the Lagrangian methodology is used, along with the assumption that the dispersed phase is dilute enough not to affect the continuous flow field (one-way coupling).

3. Particle trajectory equations

Assuming only drag is significant, the vector force balance on a particle is written as follows:

$$\frac{du_p}{dt} = F_D(u - u_p) \qquad (1)$$

where the drag force per unit mass may be expressed as:

$$F_D = \frac{18\mu}{\rho_p d_p^2} C_D \frac{\mathrm{Re}}{24} \qquad (2)$$

In the above, u is the fluid velocity, u_p is the particle velocity, μ the fluid dynamic viscosity, ρ_p the particle density, d_p the particle geometric diameter, and Re the relative Reynolds number defined as:

$$\mathrm{Re} = \frac{\rho_p d_p \left| u - u_p \right|}{\mu} \qquad (3)$$

In FLUENT, the drag coefficient is obtained from the expression:

$$C_D = a_1 + \frac{a_2}{\mathrm{Re}} + \frac{a_3}{\mathrm{Re}^2} \qquad (4)$$

where the a's are constants which apply to spherical particles for wide ranges of Re. The trajectory $L(L_x, L_y, L_z, t)$ of the particle is obtained by simply integrating the following vector equation with respect to time:

$$u_p = \frac{dL}{dt} \qquad (5)$$

In laminar flow, the above relations (1) to (5) are sufficient to compute the trajectory of individual particles, since the fluid velocity u is constant with time for steady state problems. The particle concentration and deposition is therefore computed in a deterministic Lagrangian fashion, and yields quite accurate results as shown by Healy [2]. In the presence of significant turbulence, the computation of particle motion becomes considerably more complicated because of the random velocity fluctuations which the particle faces as it is carried away by the fluid.

4. Eddy Interaction Model in FLUENT

A popular model to describe particle dispersion in turbulent flows is the so-called "Eddy Interaction Model" (EIM) developed by Gosman and Ioannides [3] and used in FLUENT. The EIM is a stochastic random walk treatment in which particles are made to interact with the instantaneous velocity field $\bar{u}$ +*u'*(t), where $\bar{u}$ is the mean velocity and *u'*(t) the fluctuating velocity. By computing the paths of a large enough number of particles, the effects of the fluctuating flow field can be taken into account. In essence, the EIM aims at reconstructing the instantaneous field from the local mean values of velocity and turbulent intensity.

The EIM models the turbulent dispersion of particles as a succession of interactions between a particle and eddies which have finite lengths and lifetimes. It is assumed that at time t_o, a particle with velocity u_p is captured by an eddy which moves with a velocity composed of the mean fluid velocity, augmented by a random "instantaneous" component which is piecewise constant in time. When the lifetime of the eddy is over or the particle crosses the eddy, another interaction is generated with a different eddy, and so forth. Based on the model of Gosman and Ioannides, the eddy has the following length and lifetime:

$$L_e = (C_\mu)^{3/4} \frac{k^{3/2}}{\varepsilon} \qquad (6)$$

$$\tau_e = C_L \frac{k}{\varepsilon} \qquad (7)$$

where *k* and ε are respectively the turbulent kinetic energy and dissipation rate, while C's are constants. In the Reynolds Averaged Navier Stokes (RANS) framework, the mean velocity $\bar{u}$ is obtained from any of the available turbulence models (*k-ε, k-ω*, RSM, etc). The value of $u'(t)$ which prevails during the eddy lifetime is randomly drawn from a Gaussian distribution. Hence, in component notation, one has:

$$u' = \lambda_1 \sqrt{\overline{u'^2}} \qquad (8)$$

$$v' = \lambda_2 \sqrt{\overline{v'^2}} \qquad (9)$$

$$w' = \lambda_3 \sqrt{\overline{w'^2}} \qquad (10)$$

where the λ's are random numbers with 0 mean and unit standard deviation, while the remainder of the right-hand side represent the local rms values of the velocity fluctuations. In the RANS modeling of turbulence, the turbulent kinetic energy *k* is one of the variables solved for. In the current version of FLUENT, the fluid velocity fluctuations used for particle tracking are assumed isotropic, and the rms values of velocity are simply obtained from the relationship:

$$\sqrt{\overline{u'^2}} = \sqrt{\overline{v'^2}} = \sqrt{\overline{w'^2}} = \sqrt{\frac{2k}{3}} \qquad (11)$$

As already mentioned, and later confirmed in the results section, relation (11) introduces a large over-prediction for the wall normal component v' in the boundary layer, and hence a more physically sound alternative will be developed in the next section.

5. Inclusion of a boundary layer model in FLUENT

In the new treatment of particle turbulent dispersion, the default model with the isotropic turbulence assumption is employed as long as the particle is outside the boundary layer, i.e. for as long as the dimensionless particle distance to the nearest wall y^+ is greater than 100 (for forced flows). If the particle crosses inside the boundary layer, then the values of the rms fluctuating velocities are modified to account for the strong anisotropic nature of turbulence. Ideally, the rms values should come from experimental or DNS data for the particular geometry and Reynolds number. In the current implementation, DNS fits for channel flow (Re=13000) obtained by Dreeben et. al [4] are used for both the rms velocities and turbulence dissipation rate:

$$u'^+ = \frac{\sqrt{\overline{u'^2}}}{u^*} = \frac{0.40 \cdot y^+}{1 + 0.0239(y^+)^{1.496}} \qquad (12)$$

$$v'^+ = \frac{\sqrt{\overline{v'^2}}}{u^*} = \frac{0.0116 \cdot (y^+)^2}{1 + 0.203 \cdot y^+ + 0.00140(y^+)^{2.421}} \qquad (13)$$

$$w^+ = \frac{\sqrt{\overline{w'^2}}}{u^*} = \frac{0.19 \cdot y^+}{1 + 0.0361(y^+)^{1.322}} \qquad (14)$$

$$\varepsilon^+ = \frac{\varepsilon}{(u^{*4}/\upsilon)} = \frac{1}{4.529 + 0.0116 \cdot (y^+)^{1.75} + 0.768 \cdot (y^+)^{0.5}} \qquad (15)$$

where u^* is the friction velocity and ν the fluid kinematic viscosity. The above represent the rms values for the streamwise, wall normal and spanwise direction, respectively. Although these fits are not universal, they are found to be only slightly dependant on the Reynolds number for predominantly two dimensional flows [5], and should therefore provide better results than the default isotropic model. The rms values of velocity are plotted in Figure 1.

In the new FLUENT model, the boundary layer modifications are made general enough so that highly 3D flows can also be tackled. Hence, at any instant during the trajectory integration inside the boundary layer, the particle distance from the nearest wall (y^+) is computed, as is the normal, streamwise, and spanwise unit vectors at the particle location. This information allows the correct assignment of the component fluctuating component velocities in equations (12) through (14), by first computing these values in the local particle-wall coordinate system which varies with particle location, then transforming theses values back to the fixed computational coordinate system.

The time integration of the trajectory equations becomes complicated very near to the wall, because the eddy lifetime (equation (7)) tends to zero, and hence very small time steps are necessary. A lower limit on the eddy lifetime is prescribed to avoid having to deal with extremely small times steps. That is:

$$\tau_e = \max(equation(7), \frac{\tau_p}{10}, 10^{-7} s) \qquad (16)$$

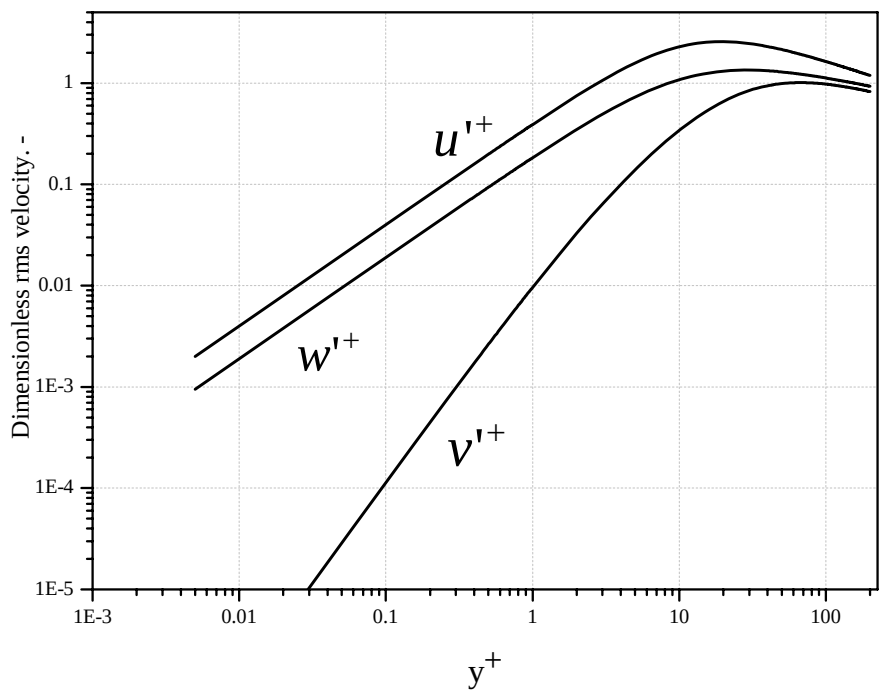

Figure 1: rms values of velocity in the boundary layer

where τ_p is the particle relaxation time representing a typical response time to changes in the carrier fluid. It is defined as:

$$\tau_p = \frac{C_c \rho_p d_p^2}{18\mu} \qquad (17)$$

where ρ_p and d_p are the particle density and diameter, respectively, μ is the carrier fluid viscosity, and C_c is the Cunningham correction slip factor which is very close to one for particles above 1 μm (those considered here). The integration time step is accordingly chosen to be one tenth of the eddy lifetime. Experimentation with smaller time steps did not show any difference in the particle deposition results.

6. Results

In the following section, the assessment of the new turbulent dispersion model is given for three different cases where experimental data on particle deposition is available: pipe flow, 90° bend flow, and a complex three dimensional internal flow. CFD Best Practice Guidelines are used to the extent possible. In particular, the solution is determined for meshes with different resolutions to insure grid independence, and higher order schemes are consistently used. In addition, all computations are performed in double precision.

6.1 Pipe Flow

6.1.1 Comparison to experiments

The deposition of particles in turbulent vertical pipe flows has been experimentally studied by a number of authors. A good test for the new model is achieved by comparing its predictions to the well known experiments by Liu and Agarwal [6]. The latter authors measured the deposition of 1.4 to 21 μm diameter olive oil particles injected in a vertical glass pipe of diameter 1.27 cm and length 1 m. Deposition data is presented for the portion of the pipe section between 0.25 m and 0.75 m, i.e. in the region where the flow is fully developed and far enough from the exit. Two sets of mean gas velocities are used, i.e. 12 m/s and 62 m/s, which correspond to Reynolds numbers of approximately 10000 and 50000, respectively. The Liu and Agarwal correlation is stated as follows:

$$V^+ = 0.0006 \cdot \tau_p^{+2} \qquad \text{for } \tau_p^+ \leq 13 \qquad (18)$$

$$V^+ = 0.1 \qquad \text{for } \tau_p^+ \geq 13 \qquad (19)$$

where V^+ is the particle deposition velocity scaled by the friction velocity. No uncertainty is given, but the data is within 30% of the values given by the correlation.

In this first simulation, two sets of 3D hexahedral meshes are generated. The second, finer mesh is obtained from the coarse mesh by simply spitting all cells except the ones adjacent to the wall into 2 in all directions, yielding 8 finer cells for any coarse cell. Because of the simple geometry and flow, the standard k-ε model is used, along with standard wall functions. The boundary conditions are a flat velocity profile at the inlet and a zero gauge pressure at outlet. After convergence with 1st order schemes is achieved, second order, then finally third order MUSCL schemes are used for all equations. The convergence is judged by monitoring the scaled residuals along with the mean wall shear stress. To judge convergence, FLUENT recommends a scaled residual of at least 10^{-3} on all variables, while simultaneously reaching stationary, iteration-independent values for some key global flow parameters (here the wall shear stress). The computation is stopped after both of these criteria are achieved. The summary of the simulations for both Reynolds numbers is shown in Tables 2 and 3. Convergence and grid independence of the results are reached.

	Coarse grid	fine grid
Number of cells	61800	352000
Mean aspect ratio	1.1	1.1
Discretization Scheme	3rd order MUSCL	3rd order MUSCL
Maximum scaled residual	3.10^{-7}	4.10^{-7}
Mean wall y+	30.1	30.1
Mean wall shear stress, Pa	0.672	0.679

Table 2: Summary information for Re=10000

	Coarse grid	fine grid

Number of cells	61800	352000
Mean aspect ratio	1.1	1.1
Discretization Scheme	3rd order MUSCL	3rd order MUSCL
Maximum scaled residual	3.10^{-7}	6.10^{-7}
Mean wall y+	135.3	129.4
Mean wall shear stress, Pa	11.91	12.00

Table 2: Summary information for Re=50000

Particle tracking is performed by releasing a large number of unit density particles which are uniformly distributed over the flow area 0.25 m downstream of the inlet. The particles are assigned the gas velocity at the time of release. Deposition over the next 0.5 m is monitored in order the replicate the conditions of the test. The number of particles chosen is 10000, as preliminary simulation with larger numbers of particles showed no change in the deposition rate beyond 5000 particles. The results of the simulations are shown in Figures 2 and 3. Several remarks can be made: first the default model gives totally erroneous predictions of the particle deposition rates, especially for the smaller particles. Given the simple geometry involved, one can justifiably conclude that the default turbulent dispersion model should not be used in wall bounded flows. On the other hand, the new model predicts reasonably well both the trends and the magnitude of deposition. For the smallest particles, the model over-predicts deposition rates. This feature is inherent to random walk models which produce the so-called “spurious drift” [7], i.e. preferential clustering of almost massless particles in low turbulence regions very close the walls. For fission product transport applications, particles are typically larger and hence the model deficiency should not have significant effects.

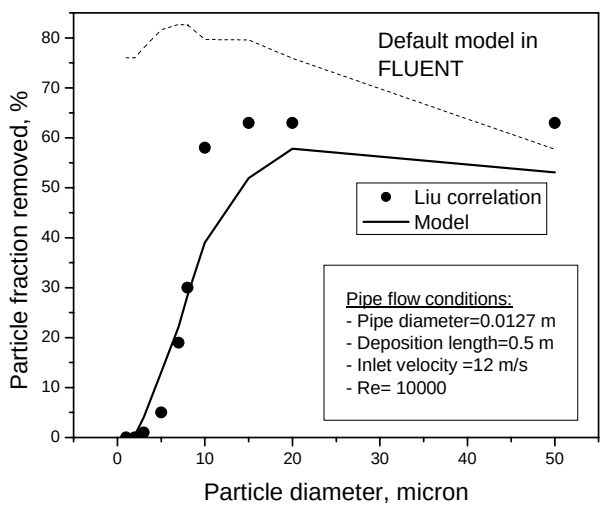

Figure 2: Particle deposition at Re=10000

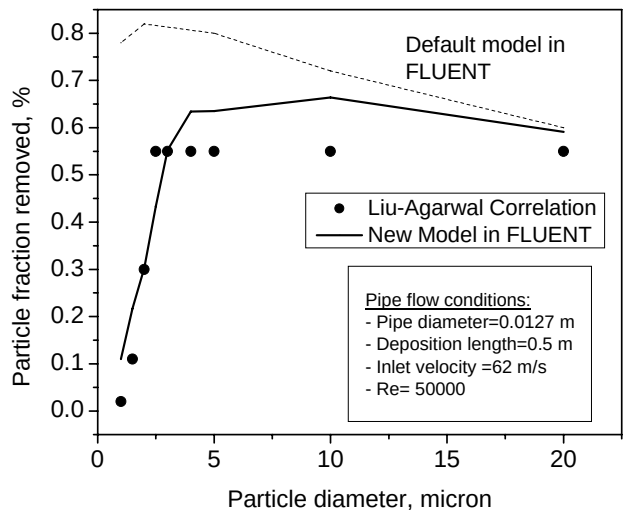

Figure 3: Particle deposition at Re=50000

6.1.2 Effect of mesh aspect ratio

To save computational resources, high aspect ratio meshes are usually used in regions where the flow details are unimportant, or else in the boundary layers. In the latter case, meshes with aspect ratios of order 50-100 are commonly used, with no detrimental effect on the flow field accuracy. In particle tracking computations, interpolation is heavily employed, because particle position rarely coincides with the nodes. To see the effect of a moderately high aspect ratio, particle tracking simulations were conducted on the 50000 Reynolds number case addressed earlier. As in the previous simulations, the mesh consists of hexahedral cells, but the mean aspect ratio is 44 this time. The summary of the simulation is given in Tables 4.

	Base case mesh	Stretched mesh
Number of cells	61800	1870
Mean aspect ratio	1.1	44
Discretization Scheme	3rd order MUSCL	3rd order MUSCL
Maximum scaled residual	3.10^{-7}	1.10^{-9}
Mean wall y+	135.3	128.1
Mean wall shear stress, Pa	11.91	11.93

Table 4: Effect of high aspect ratio mesh

As expected, the results for the stretched mesh are almost identical to those for the regular mesh, despite a cell count which is 30 smaller.

The particle tracking results are shown in Figure 4. With the high aspect ratio mesh, the agreement with the data is not as good as with the base case over most of the particle size range. Because of the considerable interpolation involved in computing particle trajectories, it is best to maintain a low aspect ratio even in boundary layer flows. One therefore should be cautious not to consider particle tracking as a mere post-processing computation performed on a grid independent flow field.

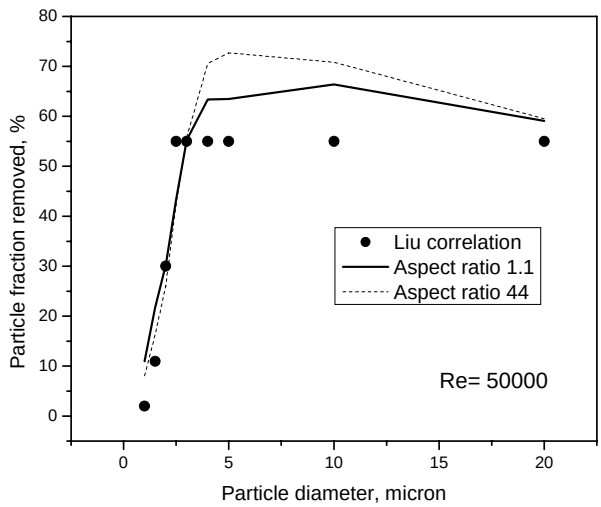

Figure 4: Effect of mesh aspect ratio

6.2 Turbulent deposition in 90° bends

Studies of deposition in bends have largely concentrated on laminar flow. To the best of the author's knowledge, the only experimental work performed in turbulent conditions is due to Pui et al. [8] who measured the penetration of particles through bends with diameters on the order of one centimeter. The authors provided the following correlation for the best fit through their data:

$$\eta = \frac{C_{out}}{C_{in}} = \exp(-2.823 \cdot Stk \cdot \theta) \qquad (20)$$

where the C's are the inlet and outlet aerosol concentrations, respectively, θ the bend angle in radians, and *Stk* the particle Stokes numbers defined as:

$$Stk = \frac{\tau_p U}{D} \qquad (21)$$

in which U is the mean gas velocity in the pipe, D is the pipe diameter, and τ_p the particle relaxation time earlier. Again no specific uncertainty is given, but the data is enveloped by the correlation within

a 30% band. A generic 90° bend section with 2 cm diameter is modeled (see Figure 5). The domain includes a straight inlet pipe with a 5 diameter developing length (in grey), as well as an exit straight section with 5 diameter length. A 10 m/s velocity boundary condition (Re=13000) is imposed at the inlet, and a 0 gauge pressure is imposed at the exit.

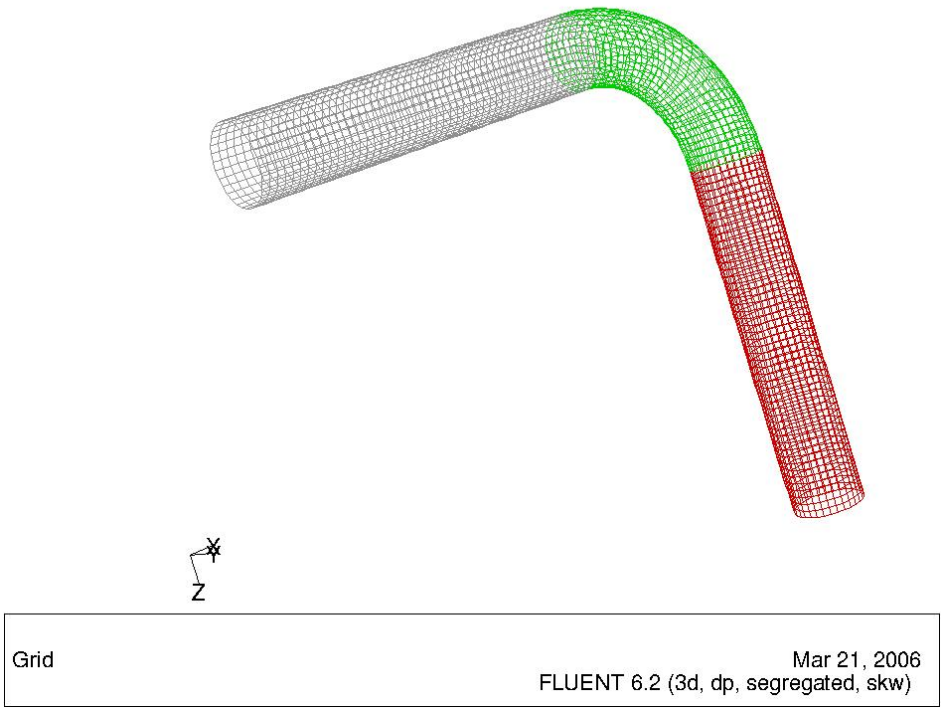

Figure 5: A view of the 90° bend section

Two hexahedral meshes are employed: a coarse mesh with 19400 cells and a fine mesh of 123000 cells. The finer mesh is obtained from the coarse mesh by halving each coarse cell direction. The cells adjacent to the walls are preserved from this procedure to maintain the y+ at approximately the same values for both meshes. The k-ω turbulence model with standard wall functions is used, since it usually performs better than k-ε in curved domains. The details of the computational case are shown in Table 5 below.

Sample velocity profiles are taken along a vertical line parallel to the Z axis (see Figure 5) which is parallel to the exit pipe. This line cuts through the symmetry plane somewhere close to the mid section of the bend. Profiles for the X velocity (X is parallel to the entrance pipe section) and Z velocity are shown in Figures 6 and 7 for both meshes. From the mean values of the shear stress as well as sample velocity profiles, one can confidently state that the computed flow is grid independent.

	Coarse grid	Fine grid
Number of cells	19400	123300
Mean aspect ratio	1.2	1.2
Discretization Scheme	3rd order MUSCL	3rd order MUSCL
Maximum scaled residual	1.10^{-9}	3.10^{-9}
Mean wall y+	29.1	29.1
Mean wall shear stress, Pa	11.91	11.93

Table 5: Summary information for bend flow case

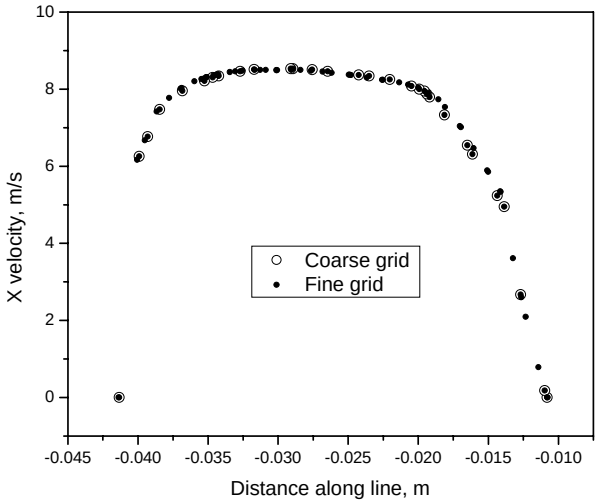

Figure 6: X velocity profile along a vertical line

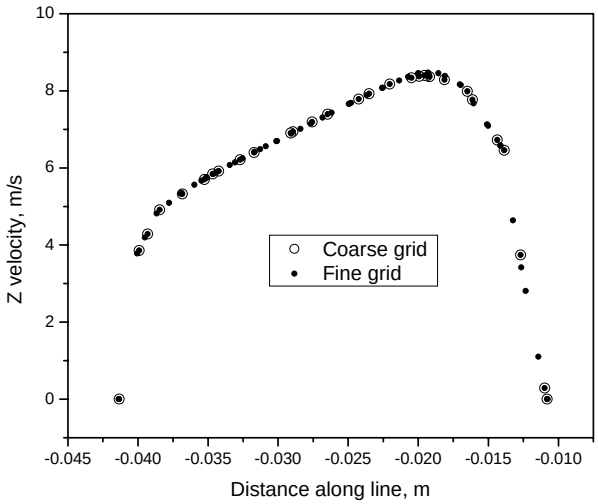

Figure 7: Z velocity profile along a vertical line

Particle tracking is conducted by releasing 10000 particles from the face which represents the entrance of the bend. Particles are uniformly distributed over the face. Comparison between the correlation and both the default and new FLUENT models is shown in Figure 8:

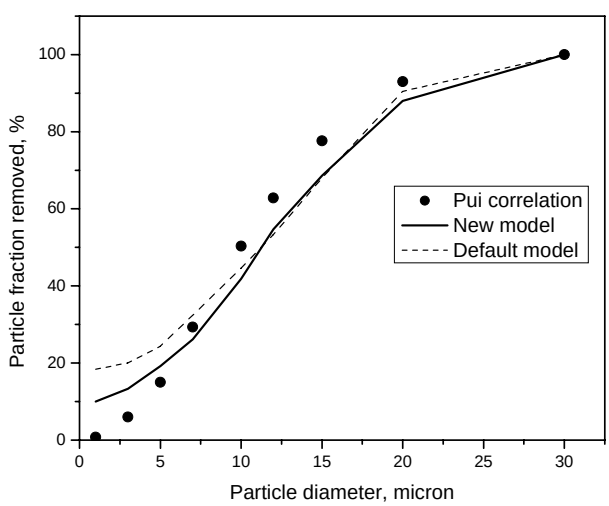

Figure 7: Particle deposition in 90° bend

As can be seen, the agreement with the data is quite good for the new model, and acceptable for the default model in FLUENT. The reasonable accuracy of the default model should however be tempered by the fact that inertial impaction is dominant over turbulent impaction for most of the particle range simulated. It can also be seen that in the lower range of particle sizes where inertia effects decrease, the new model offers better prediction thanks to the better modeling of the turbulent field in the boundary layer.

6.3 Mouth Throat Geometry

One can find only scarce data relating to particle deposition in complex three dimensional turbulent flows. Among the available data is information relative to medical aerosol removal rates in the human extrathoracic region encompassing the mouth, the pharynx, the larynx and the trachea. Aerosol deposition in those regions is unwarranted because the medication is meant for the lungs which are located further downstream. Good quality, albeit limited data was recently provided by Grigic et. al [9] who measured the removal of 3 μm, 5 μm and 6.5 μm DEHS oil particles in an idealized mouth-throat geometry. The latter was constructed from tomographic scans of many adult patients with no apparent abnormalities [10] (see Figure 9). Grigic et al. used two distinct flow rates, i.e. 30 and 90 l/min. For 30 l/min, the flow is laminar or transitional. For 90 l/min, the flow is in the turbulent range, with a Reynolds number on the order of 8000 based on the entrance diameter of 17 mm. Therefore, the particle tracking model is compared against the 90 l/min data.

Figure 9: Mouth-throat idealized geometry

Because of the complicated 3D geometry, a full tetrahedral mesh is used. The original mesh has 1.1 millions cells with a mean aspect ratio of 1.2. The cell count is relatively high in order to be able to resolve the boundary layer such that the low Reynolds number k-ω transitional flow model can be used. For theses conditions, it is required that the wall y+ be of order 1, although higher values are acceptable as long as they are within the viscous sublayer, i.e. y+ less than 5. A full grid-independence study would require running a case with close to 9 million cells, clearly outside the scope of this study.

Nonetheless, grid adaptation is performed to yield a finer grid with 2 million cells. When the solution on the latter is converged, a further adaptation produces the finest grid with 3.3 million cells. The particular adaptation procedure aims at providing higher cell resolution in regions with high velocity gradients, all the while preserving the wall y+. A flat velocity profile is imposed on the inlet face of a short 17 mm diameter pipe which provides a fully developed flow into the mouth-throat section. A 0 gauge pressure is imposed on the exit face.

	Coarse grid	Finer grid	Finest grid
Number of cells	1.1 million	2.0 million	3.3 million
Mean aspect ratio	1.2	1.2	1.2
Discretization Scheme	2nd order Upwind	2nd order Upwind	2nd order Upwind
Maximum scaled residual	6.10^{-5}	3.10^{-4}	4.10^{-4}
Mean wall y+	3.72	3.57	3.57
Mean wall shear stress, Pa	0.83	0.80	0.80

Table 6: Summary information for the mouth-throat case

A slanted line SL (see Figure 10) where the gradients are high is chosen in the symmetry plane to look at the X and Z (vertical) velocity profiles. The x and z velocity profiles are shown in Figures 11 and 12. The computation for the coarse grid is clearly not yet grid independent. The profiles for the finer and finest grids are nearly the same, in particular near the boundaries where it is especially important to have grid independence to ensure the accuracy of the particle deposition prediction. It would however be beneficial to increase the grid resolution even further to resolve the slight discrepancies which exist between the fine and finest grids in this study.

Particle tracking is performed in the finest grid with 10000 particles injected at the entrance face of the short conditioning inlet pipe. Results for the deposition fraction are shown in Table 7. As seen before, the default model largely over-predicts the deposition for all particle sizes. The new model predicts deposition rates that are within 30% of the data, which is reasonable, especially in view of the fact that the DNS fits are those of channel flows, for lack of better alternatives.

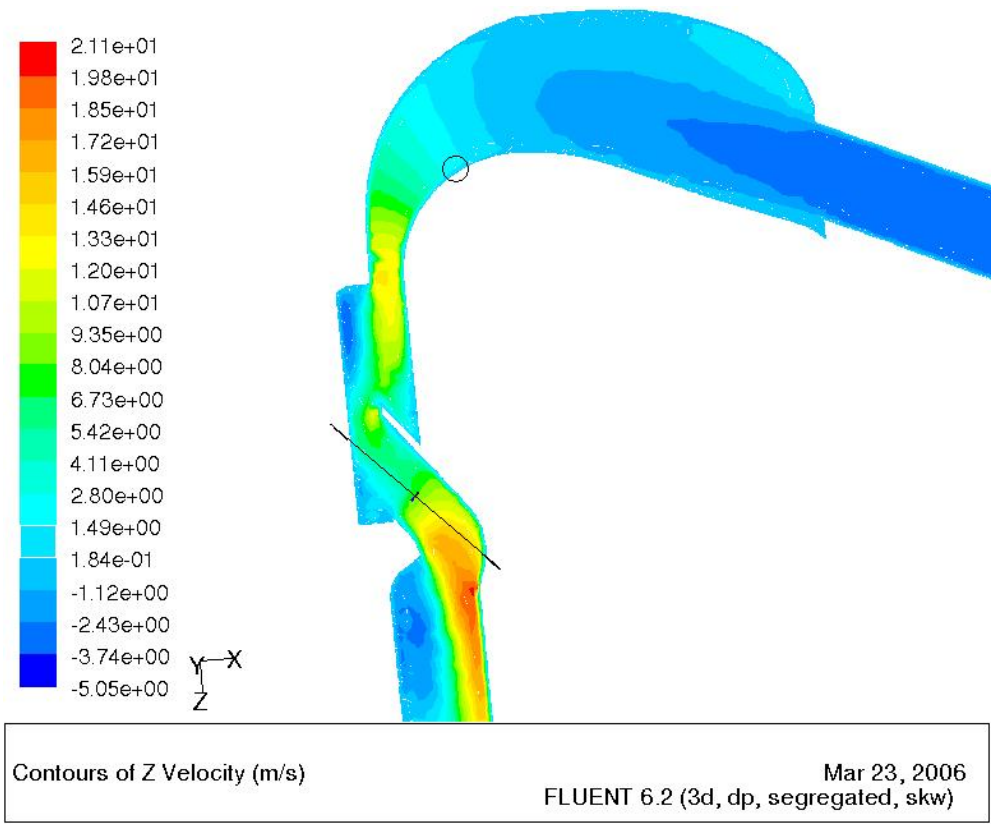

Figure 10: Slanted line (SL) along which velocity components are displayed

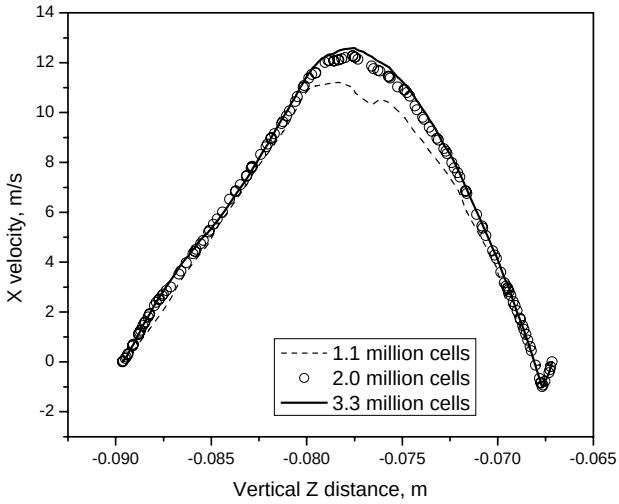

Figure 11: X velocity profile along slanted line SL

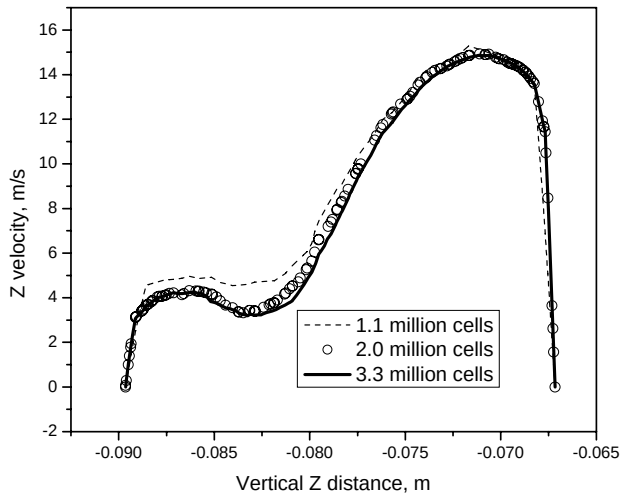

Figure 12: Z velocity profile along slanted line SL

Particle diameter, μm	Grgric data	FLUENT new model	FLUENT default model
3.0	34 ± 5	39.0	91.0
5.0	70 ± 3	48.2	94.8
6.5	80 ± 3	61.4	97.8

Table 7: Deposition fraction (%) in the idealized mouth-throat geometry

7 Conclusion

A model is implemented in the FLUENT particle tracking facility in order to specifically address boundary layer phenomena, and in particular the strong anisotropic nature of turbulence near walls. The flow field is first obtained for 2D and 3D cases using CFD Best Practice Guidelines, in particular multiple grid resolutions and higher order schemes. Particle tracking is then performed on the converged, grid-independent solutions. Comparison with experimental particle deposition rates in both 2D and 3D turbulent flows shows marked improvement over the default turbulent dispersion model.

8. References

[1] FLUENT, FLUENT 6.2 Users Guide (2005) Lebanon, USA.

[2] Healy, D.P., Young, J.B., 2001. Calculation of inertial particle transport using the Osiptsov Lagrangian method. 4th Int. Conf. on Multiphase Flow, New Orleans, Paper DJ4.

[3] Gosman, A.D. and Ioannides, E., 1983. Aspects of computer simulation of liquid fuelled combustors. J. Energy 7, pp. 482–490.

[4] Dreeben, T.D., Pope, S.B., 1997. Probability density function and Reynolds-stress modeling of near-wall turbulent flows. Phys. Fluids, 9 (1), 154-163.

[5] Antonia, R.A., Teitel, M., Kim, J., Browne, L.W.B., 1992. Low-Reynolds-number effects in a fully developed turbulent channel flow. J. Fluid Mech. 236, 579-605.

[6] Liu, B.Y.H. and Agarwal, J.K., 1974. Experimental observation of aerosol deposition in turbulent flow. Aerosol Sci. 5,145–155.

[7] MacInnes, J.M. and Bracco, F.V., 1992. Stochastic particle dispersion modeling and the tracer particle limit. Phys. Fluids A 4, pp. 2809–2824.

[8] Pui, D.Y.H, Romay-Novas, F., and Liu B.Y. H. Experimental study of particle deposition in bends of circular cross section. Aerosol Science and Technology, 7, 301-315.

[9] Grgic, B., Finlay, W.H. and Heenan, A.F., 2004. Regional aerosol deposition and flow measurements in an idealized mouth and throat. Journal of Aerosol Science 35, 21–32.

[10] DeHaan, W. H. & Finlay, W. H. 2001. In Vitro Monodisperse Aerosol Deposition in a Mouth and Throat with Six Different Inhalation Devices, J. Aerosol Med. 14, 361-367.

Acknowledgement

The author wishes to express his gratitude to Professor W. Finlay of the University of Alberta for making available the CAD files of the mouth-throat geometry.